

# RADIOMETRIC CAMERA CALIBRATION OF THE BiLSAT SMALL SATELLITE: PRELIMINARY RESULTS

J. Friedrich<sup>a,\*</sup>, U. M. Lelođlu<sup>a</sup>, E. Tunali<sup>a</sup>

<sup>a</sup> TÜBİTAK BİLTEN, ODTU Campus, 06531 Ankara, Turkey - (jurgen.friedrich, leloglu, tunali)@bilten.metu.edu.tr

Commission I, WG 6

**KEY WORDS:** Radiometric, Camera, Calibration, BiLSAT

## ABSTRACT:

The studies on radiometric camera calibration of multispectral camera of the BiLSAT satellite is presented in this work. During the study, various dark images and flat-field images have been taken, and deviations from ideal has been investigated. Various sources of error have been studied and the non-homogeneous response of the CCD is explicitly modeled. Images have been corrected according to the models and the results have been discussed.

## 1. INTRODUCTION

BiLSAT earth observing satellite has been built in the framework of a technology transfer program between SSTL, Guildford, UK and TÜBİTAK-BİLTEN, Ankara, Turkey. Since its launch on September 27<sup>th</sup>, 2003, to its sun-synchronous orbit at 686 km high, it is being operated from the ground station in Ankara. BiLSAT has a panchromatic camera with 12,6 m ground sampling distance (GSD), and four separate cameras sensitive to red, green, blue and NIR bands, together forming a multispectral camera with 27,6 m GSD.

The radiometric calibration of the cameras was not performed on the ground, so the parameters need to be estimated in-orbit. For that purpose, dark images have been obtained by imaging the Atlantic Ocean at night. Imaging has taken place in June 3<sup>rd</sup>, 2004 at 23:14:44 UTC and 23:23:29 UTC. At both imaging attempts, 5 images have been taken with 5 second intervals. For the gain calculation of images, flat-field images needed. These images have been obtained by imaging snow plateaus in Antarctica (75S 120E). The imaging campaigns for flat field images have been conducted on December 25<sup>th</sup>, 2004 at 16:07:03, January 3<sup>rd</sup>, 2005 at 11:57:29 and January 16<sup>th</sup> 2005 at 11:54:21.

In this work, a study to determine relative radiometric camera calibration parameters of BiLSAT multi-spectral camera and the first results from the study are presented.

For the absolute calibration of BiLSAT cameras, another study is being conducted for all Disaster Monitoring Constellation (DMC) satellites with the support of all satellite owners. This study is being conducted in the framework of an agreement between DMC Consortium and University of Arizona. In accordance with the agreement, test site supported by University of Arizona at Railroad Valley, Nevada, United States (38.5N 115.7E) is used and the imaging campaign took place during 3-11 July 2004. The top-of-the-atmosphere radiance values are not available yet, so the absolute calibration is not done.

## 2. CAMERA SYSTEM, ITS RADIOMETRIC BEHAVIOUR AND NOISE SOURCES

BiLSAT carries three imagers on board. The imager named ÇOBAN is out of the scope of this study, so it will not be discussed. The other two imagers are multispectral imager and panchromatic imager. The radiometric calibration study has only been made for multispectral camera, so only this imager will be discussed.

BiLSAT imagers are based on "Modular Camera" approach. The Modular Camera forms the basis of the area array camera of BiLSAT imagers. The Modular camera is a single channel unit, and is used in single configuration for a panchromatic camera, and as multiple units for a Multispectral imager. Multispectral camera is made of four physically different cameras. Multispectral imager was constructed by using four modular cameras with appropriate lenses and filters. In the modular camera, KAI 4000M CCDs were used. The specifications of the CCD are given in Table 1.

---

\* Corresponding author.

<i>Number of pixels</i>	4.2 million pixels, 2048 (H) by 2048 (V)
<i>Pixel size</i>	7.4 mm square pixels
<i>Scanning</i>	Progressive scan (noninterlaced)
<i>Outputs</i>	Four video outputs, one at each corner of the sensor
<i>Imaging area</i>	15.2 mm x 15.2 mm imaging area
<i>Shutter</i>	Electronic shutter
<i>Dark Current</i>	0.5 10 <sup>-5</sup> A/m <sup>2</sup> at 40° C
<i>Antiblooming protection</i>	Exists

Table 1. KODAK KAI 4000M CCD specifications

Band	Spectral frequency range	
	From	To
<i>Blue</i>	450	520 nm
<i>Green</i>	520	600 nm
<i>Red</i>	630	690 nm
<i>NIR</i>	760	900 nm

Table 2 Multispectral imager band spectral frequencies

As the lens of the cameras of the multispectral imager, fixed focal length LEICA APO-TELYT-R 180mm lenses with a focal length of 180mm has been used after applying modifications to make them suitable for operating in space and launch environment. The lenses have been equipped

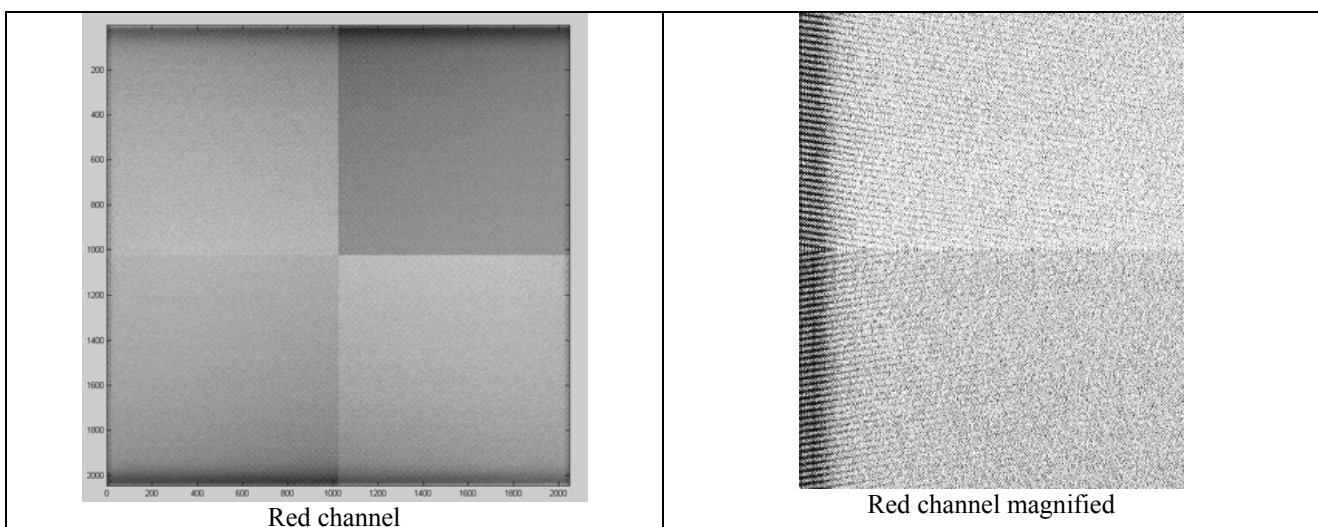
with interference filters. The filter bandwidths are given in Table 2. It can be seen that the filters were chosen to have identical spectral frequencies with that of first four bands of Landsat TM. With those technical characteristics, multispectral imager can image the earth at a 27,6m GSD and can image 56km by 56km area at a single frame.

### Dark Images

Since the CCD has four video outputs in order to speed up the reading, a single image is made up of four different images (quarters) at the beginning. When those quarters are merged, they make up a single (frame) image. Although the readout electronics for each quarter was produced to be identical with the others, due to inaccuracies of electronic components, it is not possible to make them exactly the same. These slight differences make the offset and gain settings of each quarter, slightly different from the others. The results of these differences show themselves differently in each channel. This phenomenon is evident in Figure 1 (Histogram-equalized for making patterns visible). Since these are dark images (ocean images taken at night), it can be deduced from the figures that, the average brightness of each quarter is different, mainly because of the offset differences of readout electronics. For this reason, each quarter has been treated as a separate image and corrected individually.

Another kind of noise is the sinusoidal patterns, modulating the dark images. These patterns are also visible in Figure 1. They are regarded as a modulation induced by readout electronics. When different dark images from different dates and different channels are inspected, it is seen that, every channel has its own modulation characteristic. One dark image DFT for each channel is shown in Figure 2. On the figure, the location of the noise is also shown for red band. It was interesting to observe that, the x-axis component of the noise was constant but only y-axis was changing. For the measurement of the frequencies a set of measurements has been conducted and the value of x-axis frequency was found to be 0.0878 cycles/pixel.

In one of the experiments conducted to understand the behavior of dark noise, 10 consecutive dark images were taken with 5 second intervals. The result of the analysis is shown in the Figure 1. It can be inferred from the graph that, mean noise increases as the sequence number of the image increases, but variance does not change considerably. This increase is blamed to the temperature increase of the CCD due to energy dissipation during the readout process. With the increase of temperature dark current increases and so does the noise. Naturally, it is decided to model the noise behavior of CCD as a function of temperature. But, since there is no temperature sensor to directly measure the CCD temperature, this study is postponed. Currently, the usability of other temperature sensors to find out the CCD temperature is being investigated.



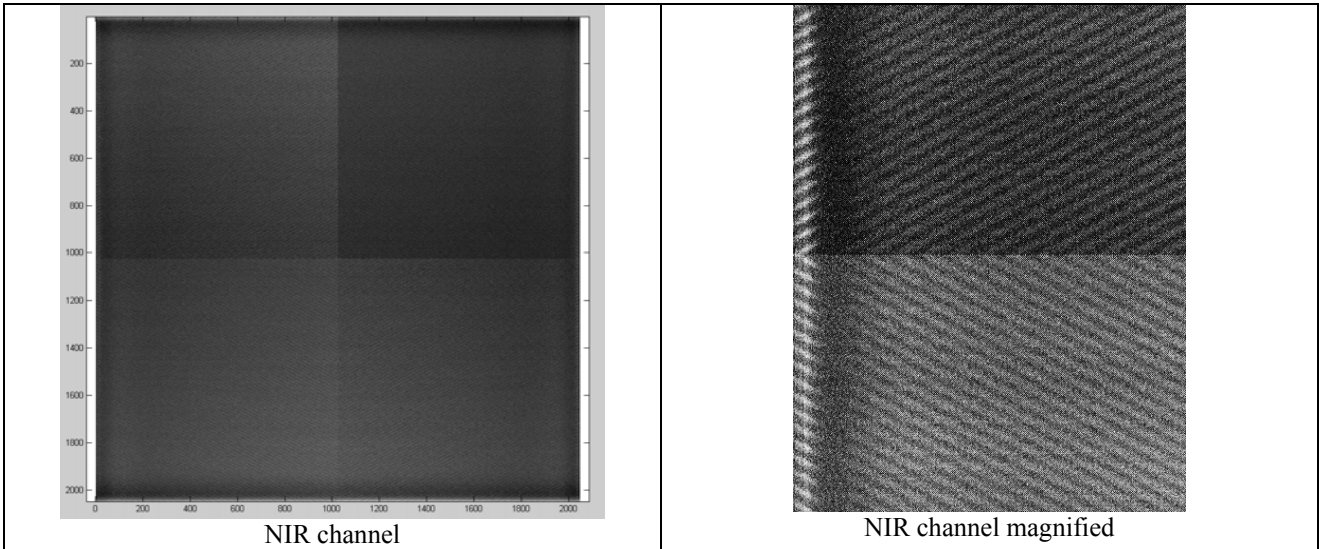


**Figure 2.** Red and NIR channels (enhanced for visibility)

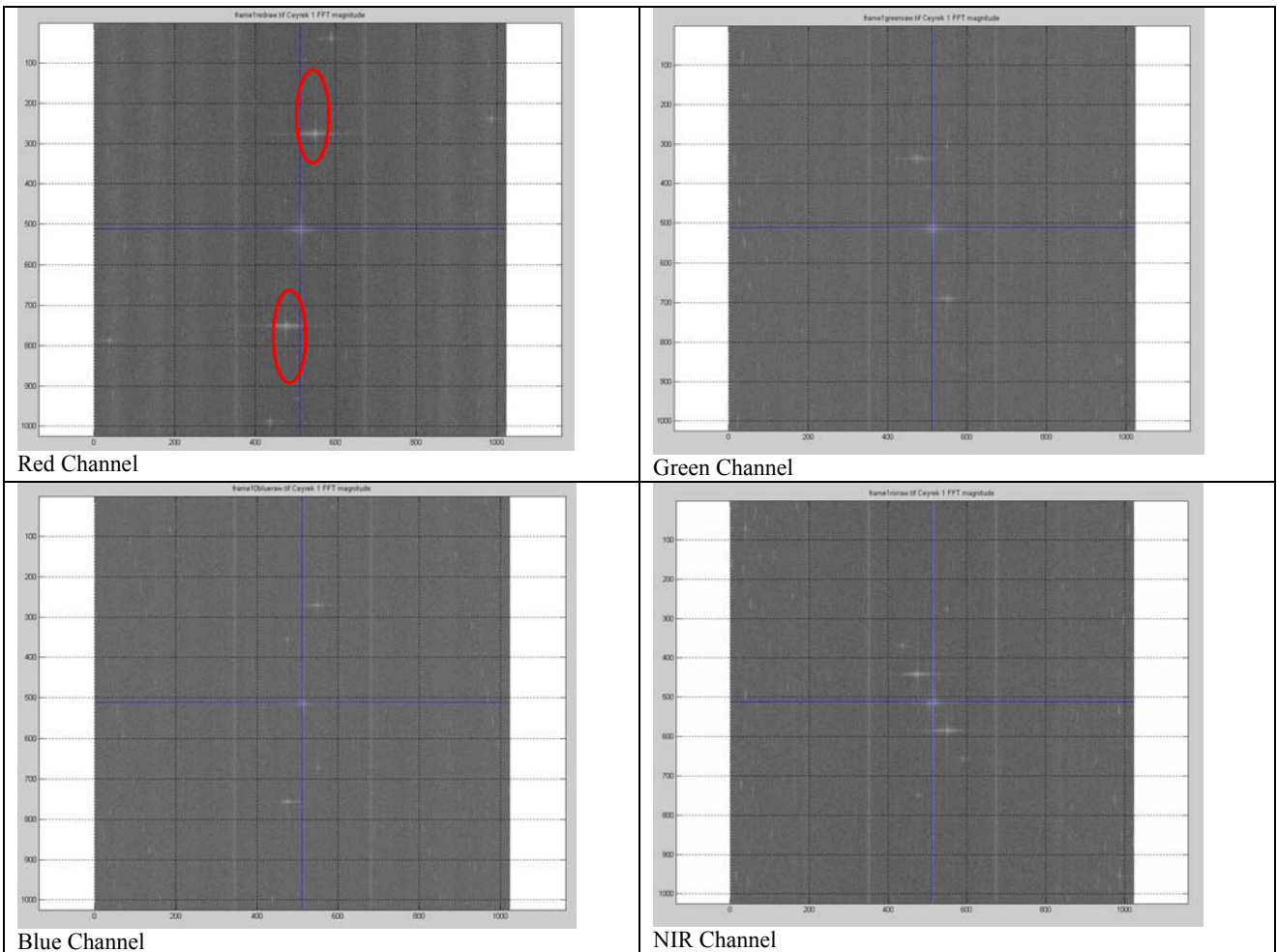


**Figure 2.** Red, Green, Blue and NIR band DFTs. For all red channel dark images, the noise lies in the ellipse in the figure

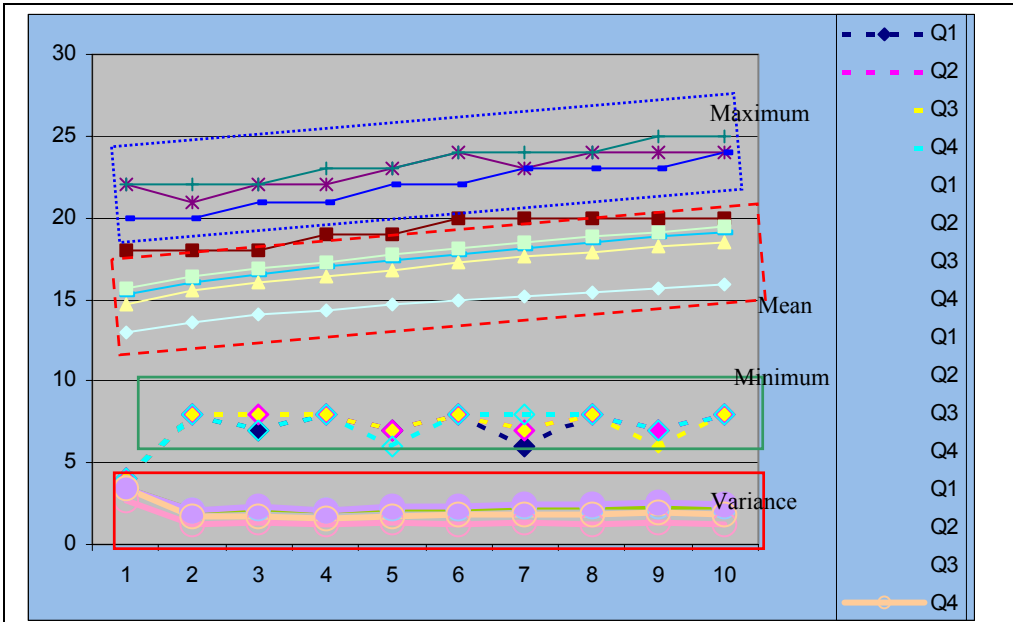


**Figure 3.** Minimum, maximum, mean and variations of 10 consecutive dark images for red channel

### Flat Field Images

For the calculation of the gain, the images of homogenous regions were needed. This need was met by imaging snow plateaus in Antarctica (75S 120E) that are widely used for that purpose. The imaging campaigns for flat field images have been conducted on December 25<sup>th</sup>, 2004 at 16:07:03, January 3<sup>rd</sup>, 2005 at 11:57:29 and January 16<sup>th</sup> 2005 at 11:54:21. An enhanced flat field image for the red band is shown in Figure 4. The borders between quarters are visible to naked eye and the brightness is decreasing as we get farther from the image center.

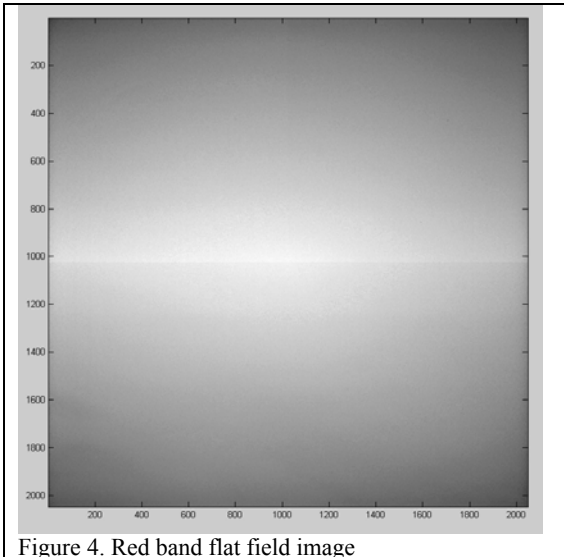


**Figure 4.** Red band flat field image

For red band images these frequencies are 0.0878 cycles/pixel for x-axis (with a variance of 0.0003) and y-axis frequency changes from 0.229 to 0.324 cycles/pixel. By using this knowledge we designed a filter in Fourier domain, to block these frequencies. The filter was based on a Gaussian filter given in Equation 1. The parameters h, k, a and b were arranged in accordance with the frequency values given above. The Fourier domain image of the filter is given in Figure 5.

$$g_{i,j} = \exp(-((i-h)^2/a^2 + (j-k)^2/b^2)/2\text{sig}^2) \quad (\text{Equation 1})$$

### 3. ERROR CORRECTION

The BiLSAT radiometric camera calibration requires at least the following corrections:

1. Removal of the periodic signal induced by readout electronics
2. Offset calculation (Dark noise modeling)
3. Gain modeling
  - a. Optical vignetting modeling
  - b. CCD pixel vignetting modeling
  - c. Other errors (Non-linearities etc.)

#### 3.1. Removal of the Readout Noise

In order to remove the periodic signal induced by readout electronics, frequency domain filtering has been used. For this purpose, various sets of dark images have been analyzed and x-axis and y-axis components of induced frequency have been measured. Measurements have shown that, x-axis component of the frequency is constant, while y-axis frequency is changing.

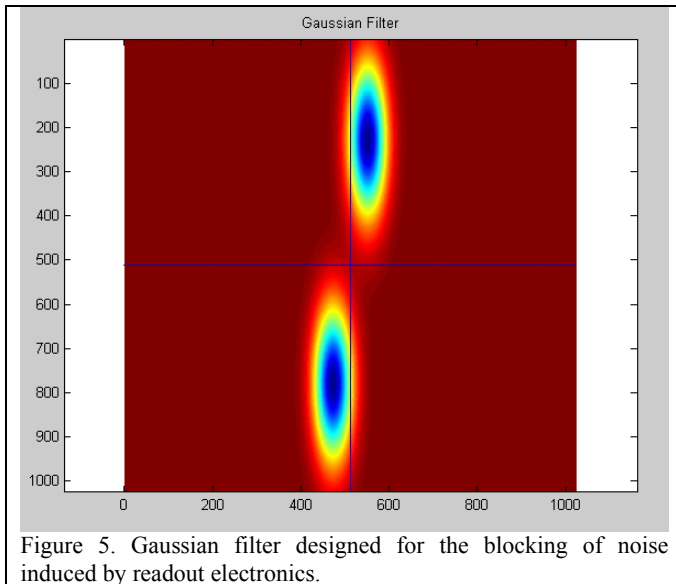


Figure 5. Gaussian filter designed for the blocking of noise induced by readout electronics.

### 3.2 Offset Calculation

Although for the correction of the dark image offset there is no need for fitting a curve, being unable to resist the attraction of expressing the dark images as a function of  $x$  and  $y$ , we tried to model the dark image after removing the sinusoidal readout noise. But, due to sharp decrease at the CCD edges (probably due to a transient response in read-out electronics), only after a 10<sup>th</sup> degree polynomial, the model had a relatively good fit with the data. So, we gave up modeling and used smoothed and averaged dark images for the offset. Some other functions can be considered for the modeling in future.

### 3.3 Gain Modeling (Flat Field Correction)

Before obtaining flat-field images, we have tried to equalize the quadrants to remove the visible borders between them. The digital values of each quadrant are modified by polynomials to minimize the least-square differences along

borderlines, but unfortunately, the borders between quarters were still visible.

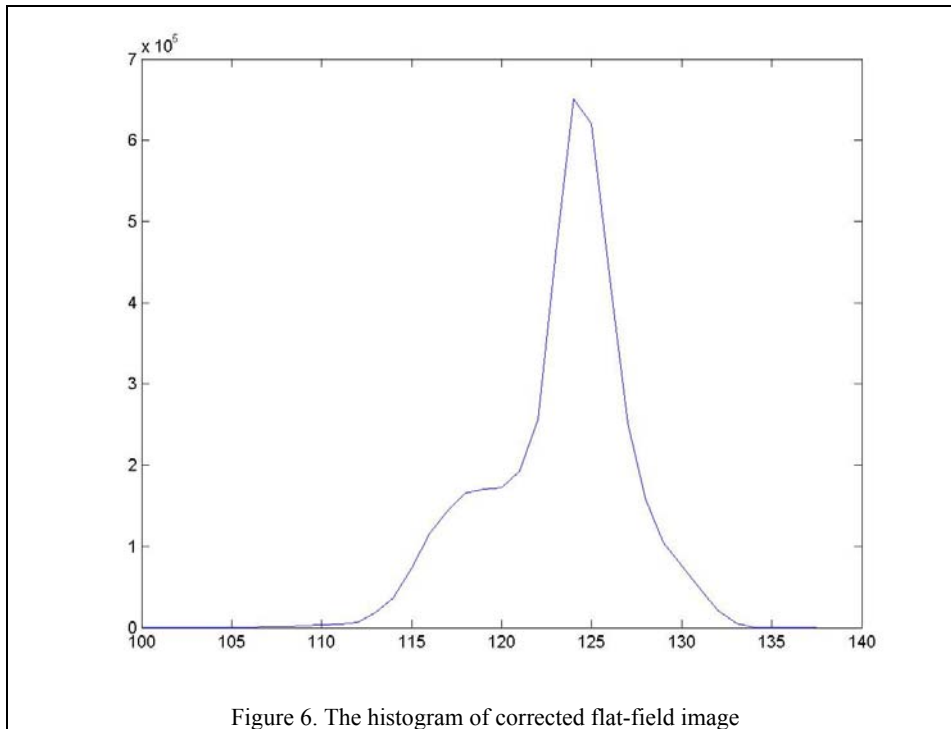
The usual and straightforward way for flat-field correction is obtaining corrective coefficients for each pixel from flat-field images and applying these coefficients to each image after removing the dark image model first. Although the blind use of flat-field correction has proved to be successful, we have tried to model the mechanism that results in non-uniform response of the CCD.

The most important source of non-uniformity is the vignetting effect. The vignetting graph of the lens used for multispectral cameras, Leica Apo-Telyt R 180mm FL  $f/3.4$ , was not available, so we could not directly correct for this effect. However, the vignetting graphs of similar lenses from the same manufacturer are examined and it was observed that a second degree polynomial approximates the function very well. So, a 3rd degree 2-dimensional polynomial should be capable of modeling the optical and mechanical vignetting with a reasonable accuracy.

For the case of pixel vignetting, the situation is a little bit more complex. The angular dependence of quantum efficiency of the CCD is available from the CCD manufacturer. The first part of these graphs can easily be approximated by a second order polynomial as well. However, this is not a function of  $r$ , but a function of angles that incoming beam of light makes with the normal of the CCD surface in vertical and horizontal directions, respectively and the angles are functions of inverse tangent of  $x$  and  $y$  over some constant. Nevertheless, the experiments showed that two 2nd order polynomials in terms of  $x$  and  $y$  are still usable.

In order to obtain an overall gain model of the images, an optimization problem has been solved. The inputs to the optimization were principle point for vignetting  $(x_0, y_0)$ , optical vignetting polynomial parameters, pixel vignetting polynomial parameters and the gain values for each quadrant.

The histogram of a flat-field image corrected using the model is shown in Figure 6. Some of the error distribution is due to random noise and non-homogeneity of the imaging targets, while remaining error is due to the model. The model will be refined using more images.



#### 4. CONCLUSIONS

This work describes the characteristics of the noise sources and radiometric behavior of multispectral camera of BiLSAT and proposes and evaluates different correction techniques. The non-homogeneous response of the CCD is explicitly modeled.

But, due to complexity of the problem, proposed techniques had limited success. In the future, some other surfaces will be tried to fit the flat-field images, not only second order polynomials. Also, the readout electronics should be investigated thoroughly and their mechanisms for adding noise should be understood well.

As noted previously, the effect of temperature on dark noise is evident from the images but there is not a sensor to directly measure the temperature of the CCD. So, some means to estimate the temperature of the CCD should be found. If this fails, by taking consecutive images at different intervals and observing the mean of dark noise, a noise model can be constructed in terms of orbital parameters, ADCS parameters and the duration since the camera is switched on.

#### REFERENCES

- Am. Soc. of Photogrammetry (1996) Manual of Photogrammetry, 4<sup>th</sup> ed., 1056 p.
- Gonzalez, R.C., Woods, R.E. (1992) Digital Image Processing, Addison-Wesley, Reading MA, 716 p.
- Koch, K-R. (1999) Parameter Estimation and Hypothesis Testing in Linear Models. Springer Verlag, 378 p.
- Mikhail, E.M., McGlone, C., Bethel, J.S. (2001) Introduction to Modern Photogrammetry, John Wiley & Sons, New York, 496 p.